Multielectron effects in the **4d** photoionization of atomic indium

M. Huttula, S. Heinäsmäki, E. Kukk, R. Sankari, H. Aksela, and S. Aksela

Department of Physical Sciences, University of Oulu, P.O. Box 3000, 90014 University of Oulu, Finland

(Received 26 April 2004; published 31 August 2004)

Observed intensity distribution in the high resolution synchrotron radiation excited 4d photoelectron spectrum of In is compared with the predictions based on the relativistic single configuration (SC) Dirac-Fock calculations. Many-electron effects beyond the SC approximation were found to cause additional fine structures in some of the photoelectron lines.

I. INTRODUCTION

The research of the electronic structure of vapor phase metal atoms was largely active in the 1970s before the inventory of modern synchrotron radiation sources and high resolution experimental equipments. Thus, the earlier data was obtained with conventional UV radiation sources such as He discharge lamps. Photoionization of the outer orbitals of indium was, to our best knowledge, last studied in 1979 by Lee and Potts [1]. They recorded the In 4d photoelectron spectrum, excited with He II radiation, but due to experimental limitations with He 1s ionization and H I excited In 5p ionization overlapping in energy with the indium 4d spectrum, the spectrum remained rather unresolved.

The electronic configuration of neutral atomic indium is $[\mathrm{Kr}]4d^{10}5s^25p^1$, i.e., In has one 5p electron above the closed shell structure. In the *LSJ* coupling scheme the atomic ground state is described as ${}^2P_{1/2}$ and the first excited neutral state as ${}^2P_{3/2}$. The excited levels can be reached with thermal excitation and the populations can be estimated using the Boltzmann distribution. In our previous work of the 4d photoionization of atomic tin [2], we were able to produce the shape of the experiment relatively well by SC calculations taking the multiple thermally excited photoionization initial states into account.

In this work we report a detailed experimental and theoretical study of the indium 4d photoionization. The photoelectron spectrum is interpreted with the aid of existing studies of In photoionization [1], autoionization [4], and optical data [3]. The transitions from both initial states are theoretically predicted with relativistic *ab initio* Dirac-Fock (DF) calculations and compared to the experiment. The electron configurations applied in our calculations correspond to single nonrelativistic configuration (SC). The many-electron effects apart from our SC predictions are discussed.

In photoionization of indium, the coupling of the 4d hole to the open 5p shell results in 12 energetically widely spread photoionization final states. Part of the $4d^{-1}$ states are energetically allowed to decay further by Auger transition. This is because the Auger final state lays between the photoionization final states, as noted from the optical data [3] and from the work of James *et al.* [4]. Similar situation occurs, for example, in Xe 4p photoionization (see Ref. [5] and references therein). The intensity of the Xe $4p_{1/2}$ photoelectron line is distributed over a large energy region due to the very

short lifetime, whereas the $4p_{3/2}$ line is redistributed into several closely lying peaks due to the strong mixing of photoionization final states with the energetically close series of two-hole one-electron states. Also in a recent study of resonant cascade Auger process in argon [6], multielectron effects were found to result in broad structures in the decay spectrum due to the mixing of Auger final state with a set of nearby lying Rydberg states. Thus, based on Refs. [5] and [6], the intensity redistribution via mixing of states would be expected to take place in indium 4d photoionization.

II. THEORY

If the bound many-electron states are described using the expansions of the atomic state functions (ASF) into configuration state functions (CSF), the photoionization cross sections can be approximatively obtained by determining the weights of initial state "parent" configurations in the final states. To be more precise, the initial state CSF is formed by coupling an electron with quantum numbers $n_\alpha l_\alpha j_\alpha$ to the parent configuration. We then assume that the core stays frozen during the ionization, which allows us to search for the final states with the same parent CSFs. The corresponding weights of the ASFs are multiplied, weighted by a coefficient depending on the angular momenta of the ground state and the ionized orbital.

With these approximations the relative Bethe-Born cross section for atomic photoionization (see the paper by Mäntykenttä *et al.* [7]) can be written, after performing the summation over angular momentum of the final photoelectron plus ion state, as

$$Q_\beta^{(i)} = \frac{1}{3}(2J_i+1)(2j_\alpha+1)$$

$$\times \left| \sum_{\nu\alpha} c_{\beta\nu} c_{i\alpha} \delta_{X_\nu Y_\alpha} \right|^2 \int |\langle jl\epsilon \| r \| n_\alpha l_\alpha j_\alpha \rangle|^2 \mathrm{d}\epsilon, \quad (1)$$

where $c_{i\alpha}$ $(c_{\beta\nu})$ denote the eigenvector coefficients of the jj-coupled initial (final) ASF. The angular momenta J_i and j_α refer to the initial state and to the ionized orbital, respectively. We have also denoted the initial state parent configuration by Y_α whereas X_ν is the same configuration in the final state.

The method leaves the ratios of the associated one-electron dipole matrix elements undetermined. When the

spin-orbit coupling in the final state is not very strong, one may express the single-electron amplitudes in the *LSJ* coupling and then select a ratio of the amplitudes corresponding to the two possible continuum waves $l=l_\alpha \pm 1$. Away from the cooper minimum, the amplitude with higher l usually dominates.

This frozen-core approximation can be used to obtain quite reliable estimates for sufficiently narrow energy regions, where the ratio of the decay amplitudes does not change appreciably. A more detailed discussion of the method in the case of closed shell atom Ba can be found in Ref. [7].

Energies and wave functions for the states involved in the transitions were generated using the GRASP92 [9] code which is based on the multiconfiguration Dirac-Fock (MCDF) method [8]. All the bound state ASF's were obtained in a single configuration approximation. The *LSJ* assigments for the states described with total *J* in GRASP92 were obtained using GRASP2 [10]. The linewidths of final states were determined using the RATIP package [11].

III. EXPERIMENT

The experiments were performed on the undulator beamline I411 [12] at the 1.5 GeV MAX-II storage ring in Lund, Sweden. The experimental setup, reported earlier [13], has been upgraded by replacing the electron spectrometer with a Scienta SES-100 electron analyzer.

A resistively heated oven was used to produce atomic indium vapor from solid indium. The temperature of the crucible in the oven was ca. $900\,^\circ$C, corresponding to the vapor pressure of 10^{-2} mbar [14] inside the crucible. The temperature was controlled with thermocouple sensors connected to the oven.

The electron spectra were measured at the "magic" 54.7° angle relative to the polarization vector, corresponding to angle-independent measurements. The photon energy of 61 eV was used in the measurements. The energy calibration of the $4d$ photoelectron spectrum was obtained by introducing Ar gas to the interaction region and recording the Ar $3s$ photolines at 29.240 eV binding energy [3] simultaneously with the $4d$ spectrum of indium. The $4d$ photoelectron spectrum was measured with 5 eV pass energy of the electron spectrometer corresponding approximately to 15 meV (FWHM) spectrometer contribution to the linewidths. The photon bandwidth was estimated to be 15 meV using the 30 μm exit slit of the monochromator. The total convoluted instrumental width, including the Doppler broadening, was estimated to be about 24 meV in full width at half-maximum. The lineshape of the experiment was found to reflect small asymmetry apart from the Voigt profile due to the non-Gaussian monochromator profile.

IV. RESULTS AND DISCUSSION

A. Experiment

In order to obtain the populations of the thermally excited initial states, the In $5p$ photoelectron spectrum was measured. The least-square fitting of the two photolines resulted
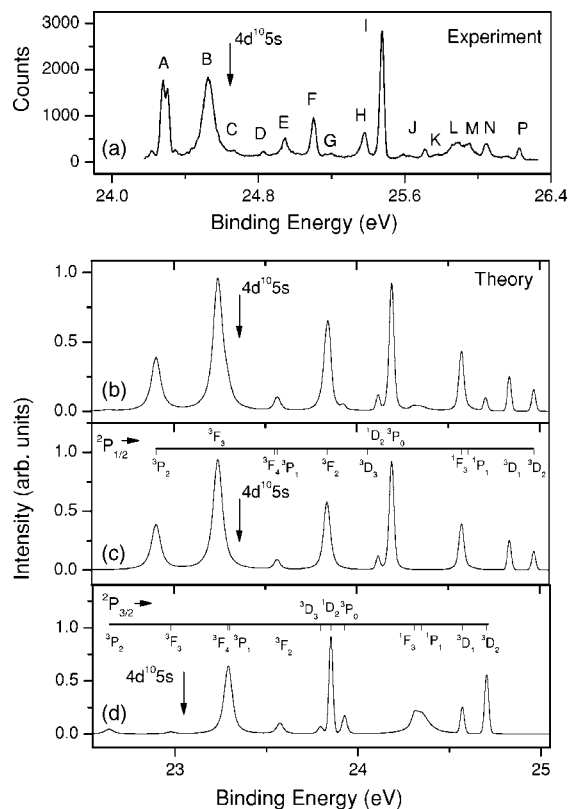
FIG. 1. The experimental and theoretical $4d$ photoelectron spectrum of In. The binding energy of the final state of the $4d^9 5s^2 5p \rightarrow 4d^{10} 5s(^2S_{1/2})$ transition is marked with a vertical arrow. The peak labels refer to Table I.

in populations of 90% for the ground electronic state $5p(^2P_{1/2})$ and 10% for the first thermally excited neutral state $5p(^2P_{3/2})$. The measured $4d$ photoelectron spectrum of atomic indium is shown in Fig. 1(a). The experimental energies, intensities, and linewidths given in Table I were obtained with least-squares fitting [15]. Table I shows also the energies obtained from the results of James *et al.* [4], where some Auger decay lines from 0 to 1 eV were assigned to have $4d^{-1}$ Auger initial states. The binding energies of the photoionized states were constructed by adding the energy of the Auger final state to the kinetic energies reported in Ref. [4]. The energies of the photolines from the thermally excited initial state $^2P_{3/2}$ were obtained by shifting the final state energies with the initial state energy separation reported in optical data [3]. As the energies of the lines D, E, F, H and I (see Table I) in our experiment match almost perfectly to the values obtained from Ref. [4], we were able to assign them to be due to the transitions from the initial states to the final states given in columns 6 and 7. Comparing our experiment to the photoionization study of Lee *et al.* [1] a good match in energy was found for the first structure A, which allowed us to assign the line to the transition $4d^{10} 5s^2 5p(^2P_{1/2}) \rightarrow 4d^9 5s^2 5p(^3P_2)$. Further assigments given by Lee *et al.* [1] are not in line with the study of James *et al.* [4]. Due to the heavy overlap with the He $1s$ ionization (He II) and In $5p$ ionization He I, further assignments in Ref. [1] were considered as unreliable or incorrect. As will be

TABLE I. Experimental and calculated energies, intensities and linewidths (Γ) of the In 4d photoelectron spectrum. Calculated energies are shifted by +1.288 eV to align the $^2P_{1/2} \rightarrow 4d^{-1}(^1D_2)$ transition with experiment. Binding energies of James *et al.* [4] are obtained adding the $4d^{10}5s$ binding energy (24.649 eV [3]) to the reported kinetic energies and applying the experimental initial state energy separation (0.274 eV [3]). Energies are given in eV and linewidths in meV, intensities are scaled to 100 for the $4d^{10}5s^25p$ $^2P_{1/2} \rightarrow 4d^95s^25p(^1D_2)$ transition both in experiment and theory. The IS and FS stands for initial and final state, respectively.

| | Experiment | | | | | | | Theory | | | | |
| | This work | | | James *et al.* [4] | | | Lee *et al.* [1] | This work | | | | |
	Energy	Intensity	Γ	Energy	IS	FS	Energy	Energy	Intensity	Γ	IS	FS
								23.926	2		$^2P_{3/2}$	$^3P_2$
A	24.3(1)	117					24.27(3)	24.19	98		$^2P_{1/2}$	$^3P_2$
								24.264	1		$^2P_{3/2}$	$^3F_3$
B	24.53	203	90					24.528	241		$^2P_{1/2}$	$^3F_3$
C	24.66(3)	15	45					24.575	20	42	$^2P_{3/2}$	$^3F_4$
				24.66	$^2P_{3/2}$	$^3P_1$		24.588	4	24	$^2P_{3/2}$	$^3P_1$
		0						24.839	0	42	$^2P_{1/2}$	$^3F_4$
D	24.83(1)	8	19	24.83	$^2P_{3/2}$	$^3F_2$	24.88(4)	24.861	3	30	$^2P_{3/2}$	$^3F_2$
E	24.95(1)	30	40	24.93	$^2P_{1/2}$	$^3P_1$		24.852	13	24	$^2P_{1/2}$	$^3P_1$
				25.01	$^2P_{3/2}$	$^3P_0$		25.083	1	17	$^2P_{3/2}$	$^3P_0$
				25.10	$^2P_{1/2}$	$^3F_2$	25.06(3)	25.125	102	30	$^2P_{1/2}$	$^3F_2$
F	25.11(1)	43	13									
				25.11	$^2P_{3/2}$	$^3D_3$	25.13	25.140	12	1	$^2P_{3/2}$	$^3D_3$
G	25.2			25.21	$^2P_{3/2}$	$^1D_2$		25.214	3	11	$^2P_{3/2}$	$^1D_2$
		0		25.28	$^2P_{1/2}$	$^3P_0$		25.347	0	17	$^2P_{1/2}$	$^3P_0$
H	25.38(1)	35	23	25.38	$^2P_{1/2}$	$^3D_3$	25.32	25.404	8	1	$^2P_{1/2}$	$^3D_3$
I	25.478(5)	100	5	25.48	$^2P_{1/2}$	$^1D_2$	25.47	25.478	100	11	$^2P_{1/2}$	$^1D_2$
								25.596	2	15	$^2P_{3/2}$	$^1F_3$
J	25.7(2)	21										
								25.632	15	93	$^2P_{3/2}$	$^1P_1$
K	25.77(2)	4	24					25.858	3	1	$^2P_{3/2}$	$^3D_1$
								25.860	46	15	$^2P_{1/2}$	$^1F_3$
L	25.9(2)	72					25.91(4)					
								25.896	7	93	$^2P_{1/2}$	$^1P_1$
M	25.95(1)	25	45					25.992	7	2	$^2P_{3/2}$	$^3D_2$
N	26.05(1)	21	40					26.125	20	1	$^2P_{1/2}$	$^3D_1$
P	26.23(1)	7	1				26.15	26.255	13	2	$^2P_{1/2}$	$^3D_2$

shown below, this is confirmed by calculations.

B. SC approximation

In the SC approximation the 4d photoelectron spectrum is due to the transitions from the two initial states $4d^{10}5s^25p$ $^2P_{1/2}$ and $^2P_{3/2}$ to the 12 $4d^95s^25p(J_\beta)$ final states according to Eq. (1). The calculated energies, intensities and linewidths are presented in Table I in columns 9, 10, 11, respectively. The SC predicted spectra are shown in Figs. 1(b)–1(d). Figures 1(c) and 1(d) present the spectra from the two initial states $^2P_{1/2}$ and $^2P_{3/2}$, respectively, and Fig. 1(b) presents the sum of the two contributions multiplied with the initial state populations. The natural linewidths given in Table I and a common 24 meV Gaussian width was used when generating

the theoretical spectra. The widths of the peaks A and B, which do not decay by Auger transition, were set to 50 meV to resemble the experiment. The origin of the "broadening" is discussed in the following chapter. Comparing the calculated sum spectrum [Fig. 1(b)] to the experiment [Fig. 1(a)] it can be noted that the overall look is very similar. All the structures assigned on the basis of earlier data [1,4] {A,D,E,F,H, and I in Fig. 1(a)} can be found from the calculated spectrum with the identification of the transitions matching to each other (see Table I). The energy splittings of the final states are relatively well predicted as the difference between calculated and experimental energy is in the order of 0.1 eV. The absolute energies are about 1.3 eV below the observed energies.

Apart from the assignments made according to the existing data, with the aid of the SC predictions we were able to

assign the other structures in the experiment; the strong broad structure B in the experiment is assigned to $4d^{10}5s^25p(^2P_{1/2}) \rightarrow 4d^95s^25p(^3F_3)$ transition and the high binding energy region, lines N and P in the experiment, can be interpreted to originate from $^2P_{1/2} \rightarrow {}^3D_1$ and $^2P_{1/2} \rightarrow {}^3D_2$ transitions, respectively. The effect of the thermally excited initial state $^2P_{3/2}$ can also be identified with the aid of our SC prediction. As already assigned based on the existing data [1,4] the minor line D in the experiment is due to the transitions from $^2P_{3/2}$ initial state to $4d^95s^25p(^3F_2)$ final state. In addition, minor structure C is assigned to originate from $^2P_{3/2}$ to $^3F_4$ and $^2P_{3/2}$ to $^3F_1$ transitions which lay close in energy (13 meV) according to our prediction and thus cannot be separated. The structures labeled J in the experimental spectrum are assigned to originate from $^2P_{3/2} \rightarrow {}^1F_3$ and $^2P_{3/2} \rightarrow {}^1P_1$ transitions. Similarly the K is assigned to be due to $^2P_{3/2} \rightarrow {}^3D_1$ transition, according to calculations. Also the very small structure G may, at least tentatively, be assigned to $^2P_{3/2} \rightarrow {}^1D_2$ transition. The experimental energy separation of the thermally excited initial states (0.274 eV) [3] was used to ensure the assignments between the initial states. The calculated intensity distribution of the $4d$ photoelectron spectrum is also in quite good agreement with the experimental findings. In Table I, for ease of comparison, the intensities are scaled to 100 for the $4d^{10}5s^25p(^2P_{1/2}) \rightarrow 4d^95s^25p(^1D_2)$ transition both in experiment and theory. With a closer look, the calculations predict the individual line intensities in the range of 75–120 % of the experimentally obtained intensity for the experimental structures labeled A,B,I,J,L,N in Fig. 1(a) which covers over 3/4 of the total intensity of the $4d$ photoelectron spectrum.

C. FISCI effects

The high binding energy part of the $4d$ photoelectron spectrum is reproduced relatively well with the SC approximation. The greatest discrepancies arise in the binding energies below 24.8 eV. Two strong structures labeled A and B in the experimental spectrum are predicted to have very small lifetime broadening since their Auger decay is forbidden. Instead of one narrow line, both structures consist of multiple peaks.

Figure 2 presents the photoionization final states, the $4d^{10}5s(^2S_{1/2})$ state and a part of the converging series of Rydberg states in an energy level diagram. The energy of the $4d^{10}5s$ configuration lies at 24.649 eV according to Ref. [3]. The energies of the higher levels in the $4d^{10}5s^1nl$ Rydberg series were extrapolated from the known level energies (Ref. [3]) using the Rydberg formula with effective quantum number and effective charge of the core. The photoionization final states $4d^95s^25p(^3F_2)$ and $4d^95s^25p(^3P_2)$ lying below the double ionization threshold $4d^{10}5s(^2S_{1/2})$ experience strong configuration interaction with the Rydberg states converging to the threshold, similar to that seen already in Refs. [5,6]. The $^3P_2$ and $^3F_3$ states overlap with a dense set of the states of the type $4d^{10}5s^1nl$, $nl=f,p$ or h Rydberg electron. Configuration interaction between $4d^95s^25p$ and $4d^{10}5s^1nl$ states gives rise to the observed multiline structure. The states which lie close in energy and have the same parity and total
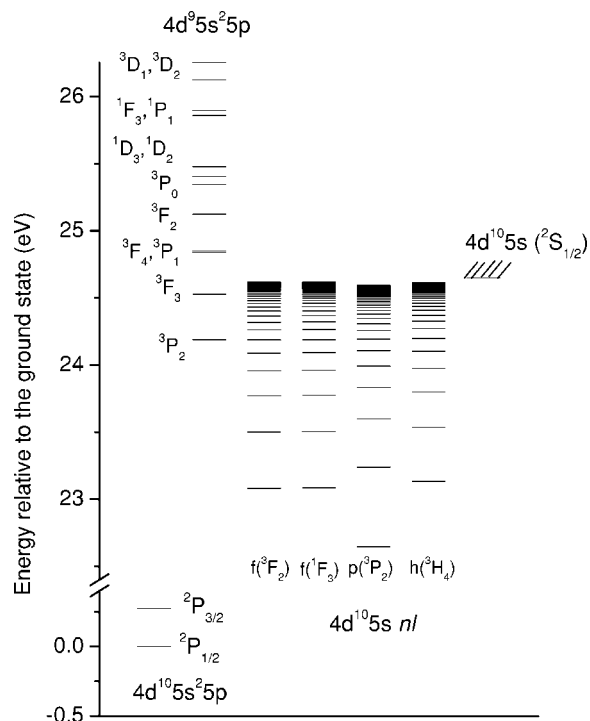
FIG. 2. The energy level diagram presenting the experimentally observed In $4d$ photoionization final states $4d^95s^25p(^{2s+1}L_J)$ and the $4d^{10}5snl$ states with $l=f,p,h$ Rydberg electron converging to the $4d^{10}5s(^2S_{1/2})$ state.

J, in case of the final state $^3P_2$ are $l=f(^3F_2)$ and $l=p(^3P_2)$ with $n=11-15$ and $n=14-19$, respectively. For state $^3F_3$ the $4d^{10}5s^1nl$ states with $l=f(^1F_3,{}^3P_3)$ and $n=16-35$ are the most probable ones to mix with. The photoionization final state $4d^95s^25p(^3F_4)$ lays just above the energy threshold of the Auger decay to the state $4d^{10}5s(^2S_{1/2})$. This transition may experience strong threshold effects. Unfortunately, due to the strong overlap with the $^2P_{3/2} \rightarrow {}^3P_1$ transition and the shoulder of line B in the spectrum, we were not able to reliably observe the intensity, the energy or the width of that individual transition.

V. CONCLUSIONS

We have reported a high resolution experimental electron spectrum of the $4d$ photoionization of atomic indium. Most of the spectral lines were interpreted with the aid of previous data [1,4]. The SC approximation was used in confirming the assignments in Refs. [1,4] and in assigning the lines arising from the thermally excited initial states. Thus we were able to assign also the minor structure seen in the experiment. In indium the threshold for the $4d^{-1} \rightarrow 4d^{10}5s$ Auger transitions lays between widely spread $4d$ photoionization final states. The SC approximation is not able to reproduce the line shapes below the Auger threshold energy which was found to be affected by many-electron effects. The photoionization final states mix strongly with the dense set of high lying $4d^{10}5snl$ Rydberg states causing dense fine structure to the lines located below the Auger threshold energy.

[1] E. P. F. Lee and A. W. Potts, J. Electron Spectrosc. Relat. Phenom. **19**, 65 (1980).

[2] M. Huttula, E. Kukk, S. Heinäsmäki, M. Jurvansuu, S. Fritzsche, H. Aksela, and S. Aksela, Phys. Rev. A **69**, 012702 (2004).

[3] C. E. Moore, *Atomic Energy Levels* (U.S. GPO, Washington, DC, 1971), Vol. 1.

[4] G. K. James, D. Rassi, K. J. Ross, and M. Wilson, J. Phys. B **15**, 275 (1982).

[5] S. Heinäsmäki, H. Aksela, J. Nikkinen, E. Kukk, A. Kivimäki, and S. Aksela (unpublished).

[6] S.-M. Huttula, S. Heinäsmäki, H. Aksela, M. Jurvansuu, and S. Aksela, J. Phys. B **34**, 1 (2001).

[7] A. Mäntykenttä, H. Aksela, S. Aksela, J. Tulkki, and T. Åberg, Phys. Rev. A **47**, 4865 (1993).

[8] F. A. Parpia, C. Froese Fischer, and I. P. Grant, Comput. Phys. Commun. **94**, 249 (1996); I. P. Grant, in *Atomic, Molecular and Optical Physics Reference Book*, edited by G. W. F. Drake (AIP, New York, 1996), Chap. 22, pp. 258–286.

[9] F. A. Parpia, C. Froese Fischer, and I. P. Grant, Comput. Phys. Commun. **94**, 249 (1996).

[10] K. G. Dyall, I. P. Grant, C. T. Johnson, and F. A Parpia, Comput. Phys. Commun. **55**, 425 (1989).

[11] S. Fritzsche, J. Electron Spectrosc. Relat. Phenom. **114–116**, 1155 (2001).

[12] M. Bässler, A. Ausmees, M. Jurvansuu, R. Feifel, J.-O. Forsell, P. de Tarso Fonseca, A. Kivimäki, S. Sundin, S. L. Sorensen, R. Nyholm, O. Björneholm, S. Aksela, S. Svensson, Nucl. Instrum. Methods Phys. Res. A **469**, 382 (2001).

[13] M. Huttula, M. Harkoma, E. Nõmmiste, and S. Aksela, Nucl. Instrum. Methods Phys. Res. A **467**, 1514 (2001).

[14] R. E. Honig, RCA Rev. **23**, 567 (1962); R. E. Honig and D. A. Kramer, *ibid.* **30**, 285 (1969).

[15] Curve fitting macro package SPANCF. http:/www.geocities.com/ekukk